Electronic structure and magnetism of Ni(100) films: Self-consistent local-orbital calculations

Xue-yuan Zhu and J. Hermanson
Physics Department, Montana State University, Bozeman, Montana 59717

F. J. Arlinghaus, J. G. Gay, Roy Richter, and J. R. Smith
Physics Department, General Motors Research Laboratories, Warren, Michigan 48090-9055
(Received 25 July 1983)

The electronic structure of three- and five-plane films of ferromagnetic Ni(100) has been computed self-consistently, with the use of an atomic-orbital basis. A surface-state band obtained for the five-plane film corresponds to surface-sensitive bands observed recently in angle-resolved photoemission measurements. Both films have a work function of 5.0 eV and an enhanced surface magnetization (ESM) compared with that of the inner planes, which have essentially the bulk magnetization. The contributions of dehybridization and band narrowing to ESM are assessed by repeating the calculations with *sp-d* matrix elements omitted. Also, while the occupancy of the *nominal d* bands decreases at the surface, their *d* character increases; cancellation of these effects explains why the *d*-orbital occupation number is nearly independent of the coordination. On the other hand, a definite surface charge transfer from *p* to *s* orbitals is observed in the calculations. We also studied Ni(100) monolayers with lattice spacings 10% smaller, and 20% larger, than the bulk spacing. In these systems also, the magnetization increases as the atomic limit is approached, while the number of *d* electrons is nearly constant.

I. INTRODUCTION

The recent surge of interest in surface magnetism of transition metals may be attributed to the development of powerful new techniques for detecting electron spin polarization at surfaces. Increasingly detailed information has been reported from spin-polarized versions of photoemission,[1–3] low-energy electron-diffraction (LEED),[4] field-emission,[5] and tunneling[6] spectroscopies. Other techniques for measuring surface magnetization include electron-capture spectroscopy,[7] the anomalous Hall effect,[8] ferromagnetic resonance,[9] and positron capture.[10] Angle-resolved photoemission[11–17] and inverse photoemission[18] measurements have provided indirect evidence of spin polarization at transition metal surfaces; a spin-polarized adaptation of the latter method has appeared recently.[19] The continuing improvement of all these techniques promises to provide a rich background of data to challenge theoretical models of surface magnetism.

Computational studies of *d*-band metal surfaces are impeded by the dual obstacles of (1) broken symmetry and (2) charge rearrangements, which must be computed self-consistently. The *d*-band systems are particularly formidable due to the simultaneous presence of localized *d* electrons and extended *sp* electrons. These difficulties are even more acute if an accurate treatment of the magnetic behavior is sought. Nonetheless, the remarkable achievements of the local-spin-density-functional (LSDF) picture[20,21,22] in providing insight into bulk magnetic behavior of transition metals[23–26] gives confidence that surface magnetism in these systems may also be amenable to calculation.

An advantage of the LSDF picture is that many-body effects are contained in a local, one-electron potential. This potential is a functional of the electron spin density. The form of the exchange and correlation terms in the potential is determined from the behavior of the free-electron gas, a system for which substantial gains have been made recently.[27,28] Ground-state properties such as the total energy, the charge density, and the magnetization may be accurately determined from the one-electron LSDF equations.[20,21] Unfortunately, the relation of the LSDF energy bands to experimental excitation spectra is less direct.[29–33] Indeed, the computed energy bands of nickel[23–26] are about 30% wider than the empirical bands,[12] and have an exchange splitting about twice the experimental value. Surface-state bands have also been measured for ferromagnetic nickel;[14–16] it is an open question whether LSDF theory can provide an adequate understanding of these states. For this reason, it is essential to perform the LSDF calculations with high precision, using the best available one-electron potential.

The first application of the LSDF approach to ferromagnetic nickel was carried out by Wang and Freeman,[34] who expanded the wave function in a minimal basis of atomic orbitals ($4s,4p,3d$), orthogonalized to the core orbitals. Because of the limited basis for the valence orbitals, the exclusion of core orbitals, and the constrained form of the potential, the method may not provide a satisfactory test of the LSDF picture. Calculations for a nine-plane Ni(100) film[34] predicted a 20% suppression of the surface magnetization compared with that of the inner planes, which had a magnetic moment near the calculated bulk value,[24] $0.58\mu_B$ per atom. A surface-induced transfer

of about 0.1 electrons from the *sp* band to the *d* band was obtained for a five-plane paramagnetic Ni(100) film[35] using the same method.

More recently, two groups[36,37] have solved the LSDF equations for Ni(100) using the linear augmented-plane-wave (LAPW) scheme. Jepsen *et al.*[36] included non—muffin-tin corrections to the charge density by expanding them in a plane-wave series. They also used an accurate $\vec{k}$-space summation technique to determine the charge densities at each stage of their iterative procedure for obtaining self-consistency. In particular, they performed a linear interpolation of the energies and wave functions obtained at 36 points in the irreducible segment of the surface Brillouin zone (SBZ); an analytic triangle method[38] was used to integrate the charge densities over the SBZ. Calculations for three- and five-plane Ni(100) films[36] showed that the surface magnetization is enhanced compared with the bulk behavior. The magnetic moments were $0.65\mu_B$, $0.58\mu_B$, and $0.61\mu_B$ per atom for the surface, subsurface, and central planes, respectively. No significant transfer of electrons from *sp* to *d* orbitals was observed at the surface; the *d*-electron occupation number was essentially constant throughout the film, with the value of about 8.3 electrons per atom.

In a later study of Ni(100) and Ni(110) films using the LAPW scheme, Krakauer *et al.*[37] obtained energy bands and magnetic moments in good agreement with Jepsen *et al.*[36] for Ni(100). In these calculations nonspherical components of the potential inside the muffin-tin spheres were omitted. Also, in their self-consistency procedure, the authors summed the charge and spin densities over only 15 points in the irreducible segment of the SBZ; they did not use the analytic triangle method[34,38] until after the last iteration was completed. Magnetic moments computed in the simple summation were 14 to 28% larger than those obtained by the analytic method. Nonetheless, the results also predict a slightly enhanced surface magnetization (ESM), and no *sp-d* charge transfer at the surface. For the Ni(110) surface, the latter authors[37] found a 13% enhancement of the surface magnetic moment compared to the bulk values and no *sp-d* charge transfer. They also found an exchange-split pair of very localized surface states in good agreement with earlier photoemission measurements.[15]

A cellular method has been applied to ferromagnetic monolayers by Noffke and Fritsche.[39] The spin density was represented as a sum of spherical atomic densities as in the method of Wang and Freeman,[34,35] but the potential was replaced by its spherical (planar) average in the atomic (empty) cells into which the film was partitioned. Computed magnetic moments for Fe, Co, and Ni(100) monolayers are larger than their bulk values; i.e., they are closer to the atomic limit, as expected. For the Ni monolayer a transfer of 0.3 electrons from the *sp* to the *d* bands—compared with the bulk configuration—is predicted. This result is contradicted by the LAPW calculations,[36,37] which obtain essentially no change of *d*-orbital occupation at the surface.

We recently extended the self-consistent local-orbital (SCLO) technique,[40] which has been successfully used to study paramagnetic *d*-band metal surfaces,[41] to include spin polarization.[42] In this method the potential *changes* during the self-consistency iterations are expanded in a Fourier series using a large number of plane waves (4200 for the monolayer). Starting matrix elements based on overlapping atomic charge densities are computed essentially exactly, in direct space. The basis set includes all occupied (core and valence) atomic orbitals as well as a set of virtual orbitals (4*p*, 4*d*, and 5*s* for nickel) for flexibility.[43] Ample testing of computational parameters such as the mesh size in real and reciprocal space, the size of the basis set, and the extent of the vacuum region between repeating slabs, has been performed.[40,42] We believe the method is sufficiently precise to test the limitations of the LSDF picture itself, given an accurate one-electron potential. Moreover, the atomic-orbital representation leads to considerable physical insight.

The spin-polarized SCLO method[42] was applied to a monolayer of Ni(100) with the bulk lattice spacing. The computed magnetic moment, $0.98\mu_B$ per atom, is 75% larger than the measured bulk value[24] of $0.56\mu_B$. This result is in good agreement with the LAPW results for the monolayer, $0.95\mu_B$ (Jepsen *et al.*[36]) and $0.86\mu_B$ (Krakauer *et al.*[37]); Noffke and Fritsche[39] obtained the value $0.90\mu_B$. We used a new exchange-correlation potential derived from a recent analysis[28] of the correlation energy of the spin-polarized electron fluid. Substitution of the von Barth—Hedin potential,[20] which overestimates correlation effects at high electron density,[28] led to a reduction of the magnetic moment by only 1%, and a reduction of the exchange splittings by 2—8 %.

Here we report calculations of the electronic structure of three- and five-plane films of ferromagnetic Ni(100). We discuss results for the work function, spin-split energy bands and densities of states, magnetic moments, and atomic-orbital occupancy. The origin of ESM in nickel is studied by switching off the hybridization interaction between *sp* and *d* orbitals; this allows us to assess the importance of dehybridization at the surface. An explanation for the observed constancy of the *d*-orbital occupation throughout the films is given. Our results are compared with state-of-the-art LAPW results and experiment. Before presenting our results, we give a brief summary of the computational method.[42]

II. METHOD

The basis set used in these calculations includes all occupied (core and valence) atomic orbitals plus a set of *s*, *p*, and *d* virtual orbitals to guarantee variational flexibility.[43] This set passes the stringent test used by other workers, that it leads to an accurate value of the work function; the latter is very sensitive to the surface-charge distribution. Since our basis of 24 functions per atom is smaller than that used in LAPW calculations[36,37] for nickel films (45 to 55 per atom), a considerable reduction of computing time is realized; see also Refs. 44 and 45. Moreover, the atomic-orbital representation provides a handy description of the results in terms that can provide important physical insight, as demonstrated below. Because the core charge density was not allowed to vary from its starting form (sum of atomic core charge densities), we do not discuss core level shifts and hyperfine fields.[37]

Because changes of the valence charge density from its initial form (overlapping atomic charge densities) vary slowly in space, and because the Coulomb interaction tends to emphasize long-wavelength components, a Fourier-transform technique was used to compute matrix-element changes during the iterations of the local density equations. The iterations were continued until all Hamiltonian matrix elements converged to within 50 meV. The Fourier integrals of the charge density were computed with an interval of 0.248 Å between real-space mesh points. In the repeating slab geometry we used, the set of plane waves needed in the Fourier series is uniquely specified[40] once the real-space mesh is defined. For the five-plane film, for example, where the repeat distance between slabs is 24.55 Å, 9900 plane waves were used.

The calculations were performed in two stages. In the first stage, carried out at General Motors Research Laboratory, the self-consistent electronic structure was determined for the paramagnetic slab. The converged Hamiltonian was then used as a starting point for the spin-polarized calculations done at Montana State University. Specifically, a trial exchange splitting was used to generate the starting potential of the ferromagnetic slab. We chose this splitting just large enough to fill the majority-spin d bands. With this choice only 20 to 30 iterations were needed to achieve self-consistency within 50 meV for all matrix elements.

The charge densities for majority- (↑-) and minority- (↓-) spin electrons were computed by summing $|\psi(\uparrow)|^2$ and $|\psi(\downarrow)|^2$ over the occupied levels at 15 and 36 special points[46] in the SBZ. The special points are the most efficient choice for evaluating the charge densities, even though they are displaced from the $\bar{\Delta}$ and $\bar{Y}$ symmetry lines, and the $\bar{\Gamma}$, $\bar{M}$, and $\bar{X}$ symmetry points in the SBZ, where the Hamiltonian matrix can be reduced to block form by symmetry considerations. The use of the special points for the $\vec{k}$-space sum permits an exact treatment[46] of the slowly varying components of $|\psi|^2$, for totally filled valence bands.

Once self-consistency was achieved we generated spin-resolved densities of states (DOS's) with a Monte Carlo sampling technique.[40] The energy bands were computed at 45 points in the SBZ and interpolated quadratically, to 20 000 or more random points. A histogram DOS, developed by counting energy levels that fell in 27-meV-wide channels, was smoothed by three-point averaging to remove some of the statistical noise. To obtain the partial DOS projected onto atomic orbitals located on specific planes, we used both the Mulliken[47] and Löwdin[48] projection techniques; these gave similar results for the localized d electrons but not the extended sp electrons. Orbital occupation numbers were determined by integrating the partial DOS up to the Fermi level E_F.

Planar charges and magnetic moments were derived by spatial integration of the charge and spin densities. Values obtained in this way differed somewhat from those obtained by adding and subtracting the orbital occupation numbers; the differences were smallest when the Löwdin[48] occupation numbers were used.

As in our earlier calculations,[42] the exchange-correlation potential was adapted from recent studies of the spin-polarized electron liquid by Vosko, Wilk, and Nusair.[28] These authors noted that the commonly used von Barth—Hedin potential[20] is inaccurate in the high-density range important in transition metals, $r_s \approx 1$ (r_s is the mean interelectronic spacing in atomic units). They used a Padé technique to interpolate accurate results for the random-phase-approximation correlation energy, valid for small r_s, to low density, where Monte Carlo results are available.[27] To determine a convenient form of the correlation potential, we first fit the paramagnetic correlation energy[28] to a simple formula. The spin-dependent correlation energy was treated in a similar fashion, and the potentials were derived by differentiation with respect to r_s and the spin polarization. In comparison with results obtained from the von Barth—Hedin potential,[20] our potential led to a 1% increase of the magnetic moment of the nickel monolayer,[42] and a 2—8 % increase of the exchange splittings. These quantities increase because the von Barth—Hedin potential slightly exaggerates the tendency for correlation to oppose ferromagnetism.[28]

III. RESULTS

A. Work function and total magnetic moment

Computed values for the work function W and total magnetic moment M are given in Table I for the one-,[42] three-, and five-plane Ni(100) films. Except for the five-plane film, both quantities were evaluated using 15 and 36 special k points[46] to determine the self-consistent potential. For the five-plane film Ni_5 we also obtained results using both $\vec{k}$-point samples but only 19 atomic orbitals per atom (the 4d orbitals were omitted); additional results, not shown, were obtained for the thinner films using the smaller basis. With the lone exception of the monolayer work function, there is no significant effect of the sampling on the results. Other workers,[36] who did not use special points[46] in their self-consistency procedure, found that a 15-point sampling is not accurate enough, even when coupled with a linear interpolation technique[38] that permits an approximate integration over the SBZ. Note that the results in Table I were obtained from a sampling of 20 000 points, after the self-consistent potential was determined using the smaller samples, as described in Sec.

TABLE I. Work function W and total magnetic moment M per unit cell for Ni(100) films. Ni_1, Ni_3, and Ni_5 denote the one-, three-, and five-plane films, respectively. Results were obtained using two $\vec{k}$-space samplings [15 and 36 special points (Ref. 46) in the irreducible SBZ] to compute the self-consistent charge and spin densities. When the 4d orbitals were omitted from the basis set, the results shown in the last row (Ni_5^*) were found.

	W (eV)		M (μ_B)	
	Number of $\vec{k}$ points			
Film	15	36	15	36
Ni_1	4.78	4.68	0.98	0.98
Ni_3	4.97	4.99	2.02	2.03
Ni_5	4.99		3.04	
Ni_5^*	5.02	5.04	2.78	2.79

TABLE II. Comparison of theoretical values for the work function of Ni(100) films obtained by several groups. The first two columns give results computed with the SCLO method; LAPW results are shown in the last two columns. The results of Arlinghaus *et al.* (Ref. 50) were computed for paramagnetic films.

	W (eV)			
Film	Present results	Arlinghaus *et al.*[a]	Jepsen *et al.*[b]	Krakauer *et al.*[b]
Ni_1	4.7	4.7	5.7	
Ni_3	5.0	5.1	5.3	
Ni_5	5.0		5.4	5.5
Ni_9		5.1		

[a]Reference 50.
[b]Reference 37.

II. We believe that our use of special points,[46] as well as the quadratic interpolation procedure, maximizes the accuracy of the calculations.

Table I shows that the work function increases from 4.7 eV for the monolayer to 5.0 eV for both Ni_3 and Ni_5. Experimental bulk values for W are 5.0 and 5.2 eV.[2,49] Agreement of this quality strongly affirms the adequacy of our basis set to represent the surface-charge distribution. The total magnetic moment, in Bohr magnetons per surface atom, increases with film thickness more slowly than the thickness itself (see Table I). This behavior implies that the moment is a decreasing function of the atomic coordination.

A comparison of results for the work function among various theoretical groups is given in Table II. Arlinghaus *et al.*[50] also used the SCLO method, but did not include spin polarization. The last two columns are LAPW results.[36,37] The major discrepancy seen in Table II is the LAPW value for the work function of the monolayer,[36] which exceeds the SCLO value by 1 eV. Also, our work function, like that of Ref. 50, increases with slab thickness, from 4.7 eV for the monolayer to 5.0 eV for thicker films, while the opposite tendency was reported in Ref. 36. This discrepancy may be due to the fact that the change of work function is determined by several factors whose effects partially cancel: band broadening, lowering of the d-band center of gravity, and surface-charge rearrangement. Note that the SCLO method predicts a work function for Cu which decreases with slab thickness.[40]

B. Energy bands of the five-plane slab

The self-consistent energy bands of Ni_5 are shown in Figs. 1 and 2 for majority- and minority-spin electrons, respectively. We further separated the bands into states that are even or odd with respect to reflection in the z axis normal to the film. The s-band minimum $\bar{\Gamma}_1$ is 8.3 eV below E_F, somewhat less than the calculated bulk value of 8.9 eV, but 73% larger than the monolayer result, 4.8 eV. Our bands are in excellent agreement with the LAPW results.[36,37]

The majority-spin d band is nearly full; the small $\bar{M}_3$ hole pocket seen in Fig. 1 contains less than 0.01 electron. The magnetization is mainly caused by the d-band holes seen in Fig. 2 for minority spin. Owing to the variations of d-orbital content (e.g., for the surface plane[51] x^2-y^2 at $\bar{M}_3$, xy at $\bar{\Gamma}_4$) among the minority-spin bands above E_F, the spin density is not spherically symmetric. Thus the exchange potential *difference* $V(\uparrow)-V(\downarrow)$ is anisotropic, producing some variation in the exchange splittings

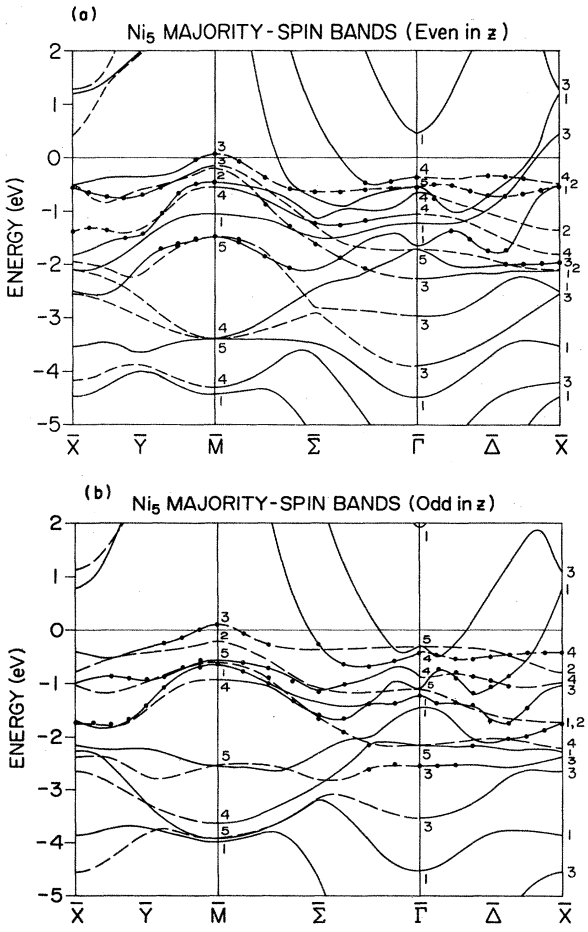

FIG. 1. Majority-spin energy bands of a five-plane Ni(100) film, in the surface Brillouin zone adopted in Ref. 42. Standard labels (Ref. 51) are used for symmetries at $\bar{X}$, $\bar{M}$, $\bar{\Gamma}$, and $\bar{X}$; symmetries along $\bar{Y}$, $\bar{\Sigma}$, and $\bar{\Delta}$ are indicated by using a solid line (dashed line) for bands with $\bar{Y}_1$, $\bar{\Sigma}_1$, $\bar{\Delta}_1$ ($\bar{Y}_2$,$\bar{\Sigma}_2$, $\bar{\Delta}_2$) characters. The bands are separated into two independent sets (odd and even) according to their reflection symmetry in the z axis normal to the film. E_F is the energy zero.

among different d orbitals.[42] Calculations which assume a spherically symmetric potential in the d-band region[37,39] cannot give a proper treatment of this effect.

As observed by other workers,[36,37] the exchange splitting increases towards the top of the d bands, since antibonding levels, e.g., the $\bar{\Gamma}_4$ (surface xy) level, have more amplitude in the region of strongest exchange potential than do bonding levels, e.g., the $\bar{M}_4$ (surface xy) level. In our calculations the exchange splitting varies from 0.4 eV at the bottom of the d band to about 0.6 eV near E_F. The majority band is narrower because its exchange potential is deeper.

C. Comparison of surface bands with angle-resolved photoemission results

Some of the bands shown in Figs. 1 and 2 have most of their probability density on the outer layer (and its mirror image). States with more than 60% but less than 80% surface character we term "weak surface states"; states with still higher surface character are termed "strong." We used solid circles in Figs. 1 and 2 to distinguish calculated states that satisfy at least the 60% criterion. These include a sizable fraction of the levels near E_F. Some of these states may evolve into bulk states as the film thickness is increased. On the other hand, some prospective surface states may only become evident for thicker films. We make no distinction between surface states and surface resonances, since the distinction is difficult to make in experiments.

Plummer and Eberhardt[14] observed two surface-state bands using angle-resolved photoemission spectroscopy (ARPS). The first band extends along the $\bar{\Sigma}$ direction from $\bar{M}$ halfway towards $\bar{\Gamma}$. Because of its dependence on the polarization of the incident light, the selection rules for ARPS (Ref. 52) imply that it is a $\bar{\Sigma}_2$ state, with odd reflection parity. Our results, like the LAPW results,[36,37] include a localized $\bar{\Sigma}_2$ band for majority spin just below E_F (within 0.8 eV), which can be assigned to the observed band.[14] Its surface character decreases from 95% at $\bar{M}$ to 60% at $\bar{\Gamma}$. This decrease is associated with the d-orbital character, which changes from x^2-y^2 ($\bar{M}_3$) to $xz-yz$ ($\bar{\Gamma}_5$). The x^2-y^2 orbital has lobes that are directed parallel to the surface plane, while the $xz-yz$ lobes point away from the plane. Moreover, the $\bar{M}_3$ state contains no atomic orbitals on the subsurface plane, by symmetry considerations;[51] thus it is effectively decoupled from the inner planes and is pushed out of the d-band continuum by the repulsive surface perturbation as a classical Tamm state.[53,54]

At $\bar{\Gamma}$, the $\bar{\Sigma}_2$ band has $xz-yz$ ($\bar{\Gamma}_5$) character, and hence much stronger overlap with "bulk" states. As a result the $\bar{\Gamma}_5$ state has much weaker surface localization[36,37] than the $\bar{M}_3$ state. Evidence has been found for the $\bar{\Gamma}_5$ state by Erskine[16] using ARPS. The behavior of the observed state with changes in the angle of incidence of the light support its identification as a $\bar{\Gamma}_5$ state. Specifically, it is strongest in s-polarized light.[16] Considerable discussion[55,56] has focused on the question of whether the $\bar{\Gamma}_5$ state explains electron spin-polarization data.[2] Our calculations suggest that the observed surface bands[14,16] near $\bar{M}$ and $\bar{\Gamma}$ can both be attributed to the $\bar{M}_3\bar{\Sigma}_2\bar{\Gamma}_5$ band shown in Fig. 1. This band was first obtained by Dempsey and Kleinman[55] using a parametrized LCAO method. The disappearance of the ARPS peak halfway to $\bar{\Gamma}$ in Ref. 14 may be explained by the progressive reduction of its surface character. Because the $\bar{\Gamma}_5$ state is so weak, it probably cannot account for the sign reversal of the electron spin polarization near threshold.[2] Our $\bar{\Gamma}_4$ state is stronger, with 90% surface character, but cannot be detected in ARPS, due to selection rules[52] (only $\bar{\Gamma}_1$ and $\bar{\Gamma}_5$ are allowed). This contradicts the assignment[36] of Erskine's ARPS peak[16] to $\bar{\Gamma}_4$ symmetry. We find no evidence for the $\bar{\Delta}_1$ minority-spin surface band near E_F invoked by Plummer and Eberhardt.[14] The observed $\bar{\Delta}_1$ emission may be due to bulklike majority-spin bands with slightly enhanced surface amplitude.

D. Densities of states

The total densities of states (DOS's) for each of the three films are given in Fig. 3. The DOS's for majority- ($\uparrow$-) and minority- ($\downarrow$-) spin electrons are essentially shifted replicas of one another, though some shape differences are caused by anisotropy of the exchange potential. The d-band widths and exchange splittings extracted from Fig. 3 are given in Table III. While the widths increase with

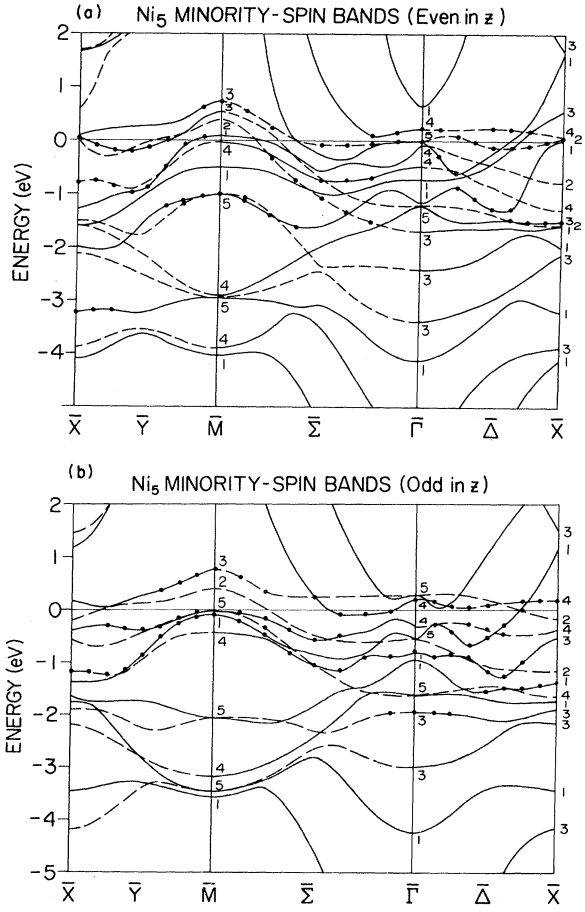

FIG. 2. Minority-spin energy bands of Ni_5, using the same conventions as Fig. 1.

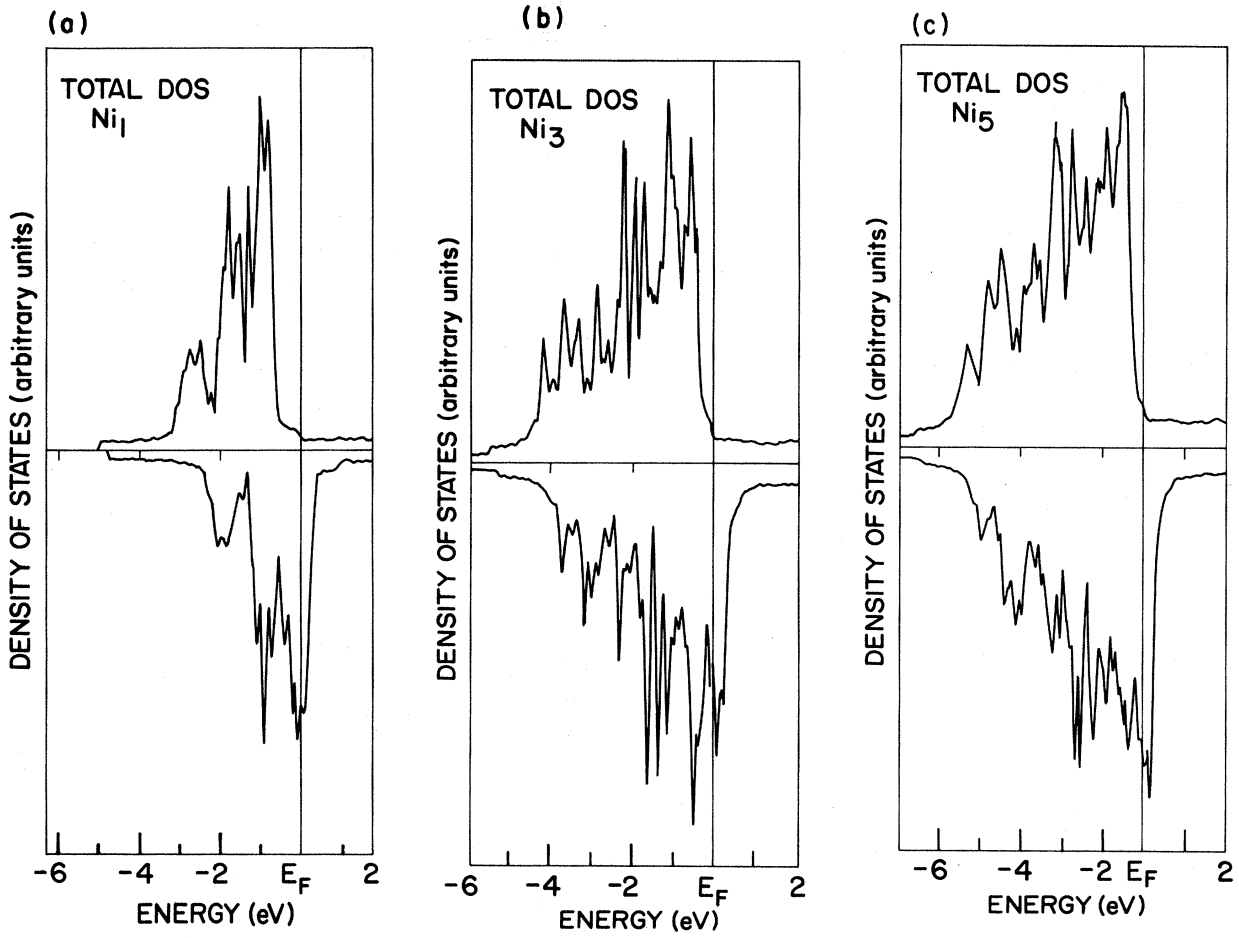

FIG. 3. Total densities of states (DOS's) for one-, three-, and five-plane films of Ni(100). E_F is the energy zero. The vertical scale is arbitrary.

film thickness, the exchange splittings decrease; both effects are due to the increased coordination. The thickest film Ni_5 has a majority-spin band width 4.6 eV and exchange splitting of 0.6 eV near E_F, in excellent agreement with the calculated bulk values[24] of 4.5 and 0.6 eV, respectively. For all three films, the exchange splitting at the top of the d bands is 50% larger than that at the bottom, due to bonding differences, as discussed above for the monolayer. As a result, the minority band is slightly wider than the majority band.

Hund's rule (full occupation of the majority-spin d bands) is obeyed exactly for Ni_1 and Ni_3. The rule is weakly broken in the case of Ni_5, for which less than 0.01 $\uparrow$-spin states are found above E_F. These holes, which decrease the magnetic moment a negligible amount, are located near $\overline{M}$ as seen in Fig. 1. Thus the magnetic moment of each film is determined by the number of $\downarrow$-spin holes in the d band. The sharpness of the DOS's above E_F implies that small errors in the Fermi-level position can lead to large errors in the magnetic behavior. An especially critical factor is the position of the s-band minimum, since this directly influences the number of d holes.

The DOS's can be projected onto the surface and subsurface planes of each film, using either the Mulliken[47] or the Löwdin[48] techniques, which give very similar results since the d-band contributions dominate. Our results for Ni_3 and Ni_5 obtained using the Mulliken analysis are given in Figs. 4 and 5. Some differences between majority- and minority-spin DOS's on a given plane can be seen. Note that the surface DOS's are somewhat nar-

TABLE III. d-band widths and exchange splittings of Ni(100) films.

Film	d-band width (eV) Majority	Minority	Exchange splitting (eV) d-band max.	d-band min.
Ni_1	3.1	3.4	0.9	0.6
Ni_3	4.3	4.5	0.7	0.5
Ni_5	4.6	4.8	0.6	0.4

rower (smaller second moment) than the DOS's of inner planes, and have a more triangular appearance. This behavior is attributed to orbitals whose lobes are directed out of the surface plane, namely the $3z^2-r^2$, xz, and yz orbitals, which are narrowed and raised by the surface potential. The DOS's of the central and second planes of Ni_5 are quite similar; this suggests that the five-plane film is sufficiently thick to reach the bulk limit at the inner planes. In fact, the central-plane DOS of Ni_3 has a rough agreement with that of Ni_5, if allowance is made for the different scales used in Figs. 4 and 5.

E. Layer-projected magnetic moments

Our results for the layer-projected magnetic moments and valence charges are given in Table IV. These were obtained by spatial integration of the self-consistent spin density and charge density; the integration region was bounded by parallel planes midway between the atomic planes. The surface values also include the contribution of the "vacuum" region. All planes are electrically neutral within 0.2%. We find that the moment increases as the coordination is reduced, from $0.61\mu_B$ at the central planes of Ni_3 and Ni_5 to $0.98\mu_B$ for the monolayer. The surface planes of Ni_3 and Ni_5 have enhanced moments, with increases of 16% and 8% compared with the center-plane values. A small oscillation of the moment is seen in the case of Ni_5, where the subsurface value dips to $0.55\mu_B$.

Two trends stand out among our results: Essentially the observed bulk magnetization,[24] $0.56\mu_B$, is found on all inner planes (even for Ni_3), and the surface magnetization exceeds that of the "bulk." The same trends also appear in the calculations of the LAPW groups summarized in Table V. Our results are in best agreement with those of Jepsen *et al.*;[36] the largest discrepancy is only 5%, for the magnetic moment at the second plane of Ni_5. This level of agreement is impressive considering that different methods were used, and the fact that the moment is the difference of much larger numbers (the majority- and minority-spin occupancies). The agreement is less striking in the case of Krakauer *et al.*,[37] though they also obtain a significant surface enhancement and bulkline behavior at the inner planes. The latter authors do not find the small dip of the second-plane magnetic moment below the central-plane result which is present in our results and those of Jepsen *et al.*[36]

A possible cause of the small discrepancies between the results of the two LAPW groups shown in Table V may be the different $\vec{k}$-space summation techniques used the calculation of the self-consistent spin density. While Jepsen *et al.*[36] used 36 points in the irreducible SBZ to compute the spin density, Krakauer *et al.*[37] used only 15. Also, while the former authors used a linear analytic triangle method[38] to improve the quality of the $\vec{k}$-space in-

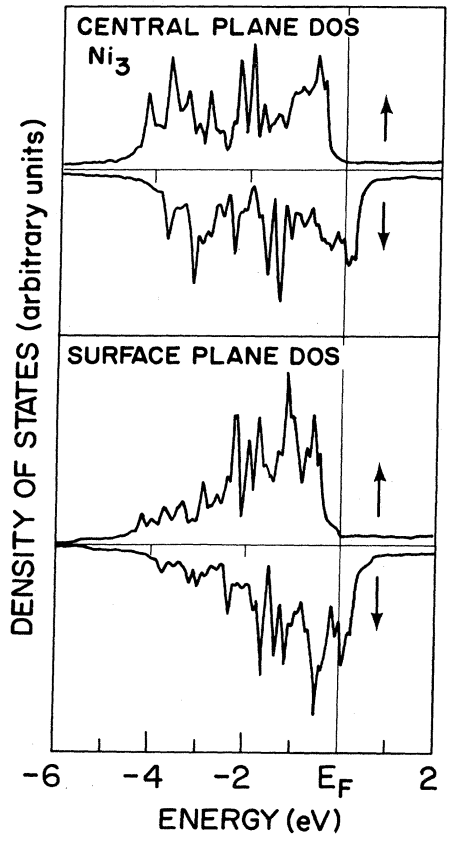

FIG. 4. Layer-projected DOS's for Ni_3, obtained using the Mulliken projection technique (Ref. 47).

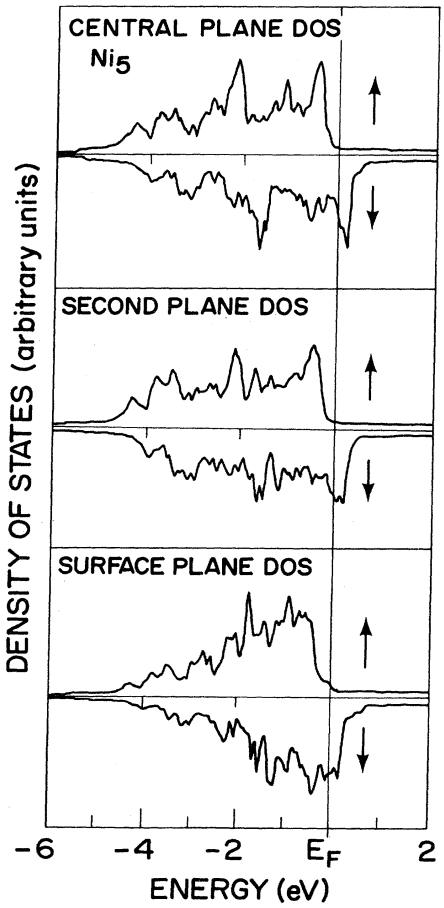

FIG. 5. Layer-projected DOS's for Ni_5.

TABLE IV. Layer-projected magnetic moments m and valence charges z for Ni(100) films. The surface layer is denoted by S, central layers by C, and the second layer of Ni_5 by $S-1$. Results obtained using two $\vec{k}$-space samplings to obtain self-consistency are shown. Results shown in the last three rows were obtained after the 4d orbitals were deleted from the basis set.

		m (μ_B)		z (electrons)	
		Number of $\vec{k}$ points			
Film	Layer	15	36	15	36
Ni_1	S	0.98	0.98	10.00	10.00
Ni_3	S	0.71	0.71	9.99	9.98
	C	0.59	0.61	10.02	10.03
Ni_5	S	0.66		10.01	
	$S-1$	0.55		9.99	
	C	0.61		10.01	
Ni_5^*	S	0.64	0.63	10.00	10.00
	$S-1$	0.48	0.49	9.99	9.99
	C	0.55	0.56	10.02	10.04

tegration at every step of the iterations, Krakauer *et al.* used this method only after the last iteration. The magnetic moments obtained by the latter authors before the analytic calculation, shown in parentheses in Table V, are 14 to 28% larger than the improved results. Nonetheless, their results also predict a surface enhancement (6% and 19%), whichever set of numbers is used.

In our approach, 15 *special* $\vec{k}$ points[46] were used to compute the self-consistent spin density. These points are chosen to maximize the efficiency of the $\vec{k}$-space summation by accounting exactly for the lowest-frequency oscillations[46] in totally filled bands. The magnetic moments we obtained before doing the Monte Carlo integration described in Sec. II are shown in parentheses in Table V. These values are only about 2% smaller than the improved results. Thus, the special-points technique[46] may be superior, even though symmetry considerations are less useful since most of the special points do not lie on symmetry points and lines. In addition, linear interpolation[38] of the energy bands may not be sufficiently accurate when it is based on only 15 points (four intervals between $\bar{M}$ and $\bar{\Gamma}$, for example; see Figs. 1 and 2). Our results, on the other hand, are based on quadratic interpolation in the last step, using 45 $\vec{k}$ points (eight intervals between $\bar{M}$ and $\bar{\Gamma}$).

Earlier results[34] for Ni_9 predicted a 20% decrease of the surface magnetic moment compared with the central-plane value. This result, which is contradicted by the results of three groups shown in Table V, may be due to the artificial constraint on the form of the charge density, or the limited basis set. Although we also used an atomic-orbital basis, we included the core orbitals and a larger set of virtual orbitals. As seen in Tables I and III, omission of the 4d orbitals leads to a reduction of the magnetic moments, without violating the surface enhancement. In any case, our excellent agreement with Jepsen *et al.*[36] demonstrates the adequacy of our basis set.

F. Orbital occupation numbers

Occupation numbers for s, p, and d orbitals on each plane are given in Table VI. Although we computed these quantities using both the Löwdin[48] and Mulliken[47] projections, we focus here on the Löwdin analysis since it leads to better agreement with the planar charge in Table IV. The Mulliken occupation numbers are less meaningful, particularly for the extended sp electrons.[57] The distribution of valence charge among the s, p, and d orbitals of each plane shows some interesting regularities. The s-

TABLE V. Comparison of layer-projected magnetic moments of Ni(100) films computed by several groups. Values given in parentheses were obtained using discrete $\vec{k}$-space summation techniques; these results were improved by approximate integration of the self-consistent spin density over the SBZ, as described in the text.

		m (μ_B)			
Film	Layer	Present results	Jepsen *et al.*[a]	Krakauer *et al.*[b]	Noffke and Fritsche[c]
Ni_1	S	0.98 (0.98)	0.95	0.86	0.90
Ni_3	S	0.71 (0.75)	0.69		
	C	0.61 (0.64)	0.59		
Ni_5	S	0.66 (0.65)	0.65	0.64 (0.73)	
	$S-1$	0.55 (0.54)	0.58	0.55 (0.68)	
	C	0.61 (0.60)	0.61	0.54 (0.69)	

[a]Reference 36.
[b]Reference 37.
[c]Reference 39.

TABLE VI. Layer-projected occupation numbers for s, p, and d orbitals. The SCLO results were found using the Löwdin projection technique (Ref. 48); values in parentheses are the Mulliken projections (Ref. 47). The LAPW occupation numbers do not include contributions outside the muffin-tin spheres (Ref. 37). The results of Refs. 36 and 37 are very similar, although the former authors do not give separate values for n_s and n_p.

		n_s		n_p		n_d	
Film	Layer	SCLO	LAPW[a]	SCLO	LAPW[a]	SCLO	LAPW[a]
Ni_1	S	0.89 (0.98)	0.42	0.30 (0.29)	0.15	8.77 (8.73)	8.26
Ni_3	S	0.70 (0.84)		0.44 (0.42)		8.81 (8.66)	
	C	0.59 (0.93)		0.54 (0.57)		8.79 (8.61)	
Ni_5	S	0.70 (0.84)	0.43	0.44 (0.42)	0.29	8.84 (8.68)	8.29
	$S-1$	0.59 (0.89)	0.46	0.53 (0.55)	0.42	8.82 (8.64)	8.29
	C	0.58 (0.80)	0.46	0.52 (0.53)	0.43	8.74 (8.55)	8.28

[a]Reference 37.

orbital occupation number n_s increases as the coordination is reduced, from 0.58 at the central plane of Ni_5 to 0.89 for the monolayer. The subsurface planes of Ni_3 and Ni_5 have nearly identical values of n_s, while the corresponding surface values are identical, at 0.70. On the other hand, n_p decreases as the coordination is reduced, from 0.54 at the center of Ni_3 to 0.30 for the monolayer. The inner-plane values are in good agreement with one another, and the surface planes of both Ni_3 and Ni_5 have identical values of n_p, 0.44. Our results show that there is a significant transfer of charge from p orbitals to s orbitals at the surface of Ni(100).

The number of d electrons n_d is almost independent of the coordination for the films studied. This conclusion is reached whether the Löwdin[48] or Mulliken[47] analysis is used, though the absolute values of n_d differ somewhat: n_d is about 8.8 and 8.7 in the two cases. Because we did not include core projections of the valence wave functions in Table VI, the total number of electrons per atom is less than 10.

Our results for n_s, n_p, and n_d are compared with muffin-tin projections cited by Krakauer *et al.*[37] Table VI shows that the LAPW values are always smaller than ours, since charge outside the muffin-tin spheres is not included. One expects large differences for s and p orbitals, but even the d-like charge is underestimated, by about 6%, in the LAPW results.[37] Nonetheless, constancy of n_d is also obtained by the LAPW workers, as well as a tendency, somewhat exaggerated, for n_p to decrease as the coordination is reduced. The s-like charge within the muffin-tin sphere decreases at the surface in the latter calculations,[37] due to the expansion of the charge into the vacuum; this is opposite to the behavior we found for n_s.

G. Influence of hybridization and band narrowing on the surface magnetism and orbital occupancy

The SCLO method can be used to explain two trends noted above: (1) the enhanced surface magnetism of the Ni(100) films, and (2) the constancy of the d-orbital occupancy n_d over all planes. These trends are common to all state-of-the-art calculations within the local-density approximation. Three factors could contribute to (1) and (2): charge transfer between layers, dehybridization, and band narrowing. Charge transfer is negligible in our calculations, since all layers are essentially neutral. Dehybridization, the increase of d character near the surface, increases both the magnetic moment m and n_d.

The effect of band narrowing is more subtle, since both the d and sp bands must be considered, and charge can flow between them, producing electrostatic shifts.[37] Unless the sp band changes its shape, or its position relative to E_F (i.e, unless the sp occupancy changes), d-band narrowing cannot change the number of d holes without violating charge neutrality. Then m cannot change either, provided Hund's rule is obeyed (full occupation of the d band, so m is approximately given by the number of d holes). Of course, the sp band also narrows and shifts. Because the sp electron gas exerts a positive pressure on the "box" of neighboring atoms which confines it, reducing the coordination tends to increase the sp occupation. As a result, n_d decreases at the surface, leading to ESM.

When dehybridization and band narrowing are considered together, the following picture emerges. Both effects increase m at the surface, but n_d remains almost unchanged due to a cancellation: sp-band narrowing leads to a decrease of n_d, dehybridization to an increase. This picture can be quantitatively verified in the SCLO method by omitting hybridization matrix elements in an auxiliary electronic structure calculation; thus the effects of dehybridization and band narrowing can be decoupled. To do this, we first transformed the self-consistent Hamiltonian into the Löwdin representation,[48] in which the basis functions are symmetrically orthogonalized Bloch functions. Then we set the sp-d matrix elements equal to zero and recomputed the magnetic moments and orbital occupancies. Our results are given in Table VII; quantities computed in the absence of hybridization are denoted with a superscript. As expected, n_{sp}^0 increases with reduced coordination, due to band narrowing. For Ni_5, n_{sp}^0 is 0.71 and 0.72 on the inner planes, and 0.80 at the surface. As predicted by Hund's rule, m^0 is nearly equal to n_{sp}^0, which is essentially the number of d holes. Hund's rule is well obeyed in these films: $n_{d\uparrow}^0$ is very close to 5 on all layers (see Table VII).

Our analysis also explains the constancy of n_d over all planes. Hybridization reduces the number of d electrons of either spin by transferring d character above E_F. The

TABLE VII. Occupation numbers and magnetic moments computed in the absence of *sp-d* hybridization, as described in the text. f_d is the ratio n_d/n_d^0, essentially the fractional *d* character of the *nominal d* bands.

Film	Layer	n_{sp}^0	n_d^0	m^0 (μ_B)	$n_{d\uparrow}^0$	f_d
Ni_1	*S*	1.02	8.95	1.06	5.00	0.980
Ni_3	*S*	0.82	9.12	0.88	5.00	0.966
	C	0.75	9.25	0.76	5.00	0.951
Ni_5	*S*	0.80	9.07	0.88	4.97	0.974
	S − 1	0.72	9.31	0.68	4.99	0.948
	C	0.71	9.27	0.71	4.99	0.942

ratio n_d/n_d^0 measures this effect (see Table VII). Our results verify the expected dehybridization at reduced coordination: n_d/n_d^0 increases from 0.942 at the center of Ni_5 to 0.974 at the surface (the largest value of this ratio is found for the monolayer, 0.980). This effectively cancels the decrease of n_d^0 at the surface caused by *sp*-band narrowing. As a result, n_d is nearly constant, at about 8.8 on all planes.

The relative importance of *sp*-band narrowing and dehybridization as influences on the magnetic moment is seen most clearly in Fig. 6, which shows *m* and n_{sp}^0 versus the coordination number [this is equal to 4 for the monolayer and 8 (12) for the surface (inner planes) of the thicker films]. The increase of n_{sp}^0 in Fig. 6 as the coordination is reduced is due to band narrowing, while the difference between n_{sp}^0 and *m* is mainly due to hybridization. Both factors contribute appreciably to ESM. In the atomic limit the effects of band narrowing and dehybridization are maximized, and the moment should be $2\mu_B$. The local-density equations apparently do not give this limit correctly;[58,59] the atomic ground-state configuration is predicted to be d^9s^1 rather than d^8s^2.

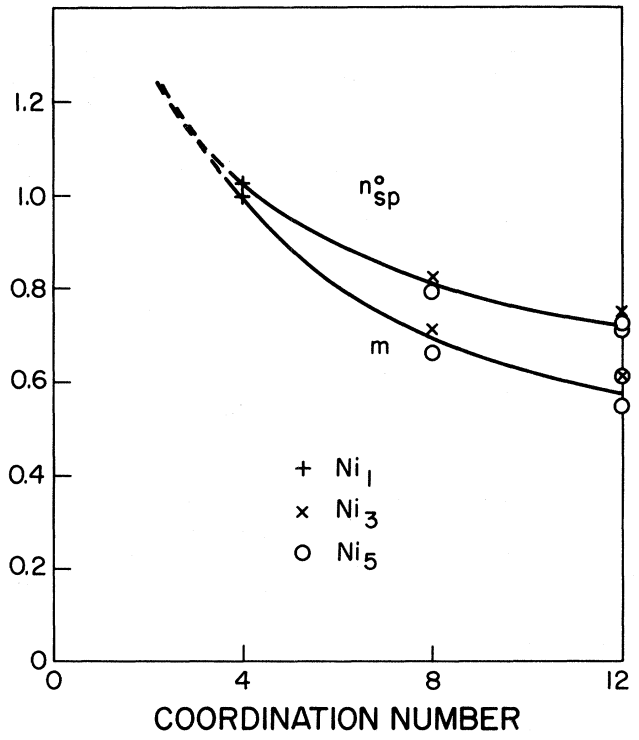

FIG. 6. The magnetic moment *m* (μ_B/atom) and *sp* occupation number n_{sp}^0 (electrons/atom) vs the coordination number (the number of nearest-neighbor atoms). The coordination number is 4 for the monolayer, 8 for the surface planes of Ni_3 and Ni_5, and 12 for the inner planes; the value for an atom in the bulk metal is also 12. To compute n_{sp}^0 we set the *sp-d* matrix elements of the self-consistent Hamiltonian equal to zero.

H. Behavior of a nickel monolayer when the lattice parameter is varied

Another context in which the effects of hybridization and *sp*-band narrowing can be studied is the monolayer with a varying lattice parameter (roughly speaking, increasing the distance between atoms is equivalent to a decrease of the coordination). The atomic limit but not the bulk limit can be achieved in this way. We did complete self-consistent calculations of the electronic structure and magnetism of monolayers with lattice constant equal to (1) the bulk lattice spacing *a*, (2) 0.9*a*, and (3) 1.2*a*. In cases (2) and (3) the calculated energy bands expand and contract, respectively, with almost no other shape changes relative to case (1). The exchange splittings decrease (increase) for the compressed (stretched) monolayer. The details are given in Table VIII. The DOS's of the altered monolayers, given in Fig. 7, are stretched and compressed replicas of the monolayer DOS's given in Fig. 3.

Orbital occupation numbers of the monolayers, comput-

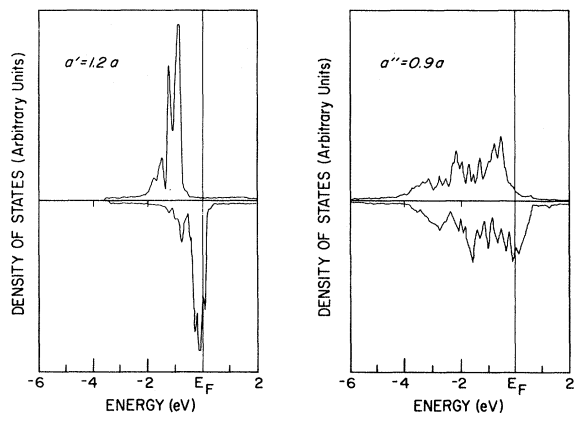

FIG. 7. DOS's of Ni(100) monolayers with lattice spacings equal to 0.9*a* and 1.2*a*, where *a* is the bulk spacing.

TABLE VIII. *d*-band widths and exchange splittings of Ni(100) monolayers with lattice spacings of $0.9a$, $1.0a$, and $1.2a$, where a is the bulk lattice spacing.

Lattice spacing	*d*-band width (eV) Majority	Minority	Exchange splitting (eV) *d*-band max.	*d*-band min.
$0.9a$	5.0	5.2	0.7	0.5
$1.0a$	3.1	3.4	0.9	0.6
$1.2a$	1.3	1.6	1.0	0.7

ed by the Löwdin projection technique,[48] are given in Table IX, together with the magnetic moment. As in Table VI, n_d remains essentially fixed at 8.8 electrons, while a charge transfer occurs from p to s orbitals as the atomic limit is approached by increasing the lattice parameter. The magnetic moment increases with the lattice parameter, from $0.80\mu_B$ for the compressed monolayer to $1.08\mu_B$ for the stretched monolayer.

We repeated the calculations after setting the *sp-d* matrix elements in the Löwdin representation equal to zero; the results are given in Table X. Here n_{sp}^0 increases and n_d^0 decreases as the atoms are separated; m^0 also increases. The moment is almost equal to n_{sp}^0, except in the compressed monolayer, where m^0 and n_{sp}^0 disagree by 17%. The latter can be explained by noting that Hund's rule is not obeyed for the compressed monolayer (see Fig. 7). Table X shows that $n_{d\uparrow}^0$ is only 4.91 in this case, while the other monolayers have almost exactly 5 electrons in the *d* band.

The ratio n_d/n_d^0, which measures the hybridization effect, is also given in Table X. It varies from 0.976 to 0.988 as the interatomic distance is increased. This increase cancels the corresponding decrease of n_d^0, so n_d is 8.8 for all three monolayers. Because n_d/n_d^0 is so close to unity, dehybridization plays a minor role in the increase of m with a. Instead the major factors are (1) *sp*-band narrowing, which increases n_{sp}^0 and hence the number of *d* holes and (2) the filling of majority-spin *d* holes as the lattice constant is increased from $0.9a$ to $1.0a$.

IV. SUMMARY

We have achieved an accurate self-consistent calculation of the electronic structure and magnetism of Ni(100) films using an atomic-orbital basis. The computed work functions and magnetic moments, both extremely sensitive to basis set restrictions, are in excellent agreement with previous LAPW results.[36,37] Our approach possesses a twofold advantage: (1) the calculations are very efficient, due to the small basis, and (2) the atomic-orbital picture provides an intuitive framework that has proven useful in drawing physical insight out of the numerical results.

In agreement with earlier workers,[36,37] we find that three- and five-plane films of Ni(100) show an enhanced surface magnetism compared with the "bulk" behavior exhibited by the inner planes. Also, the *d*-orbital occupancy is essentially independent of the distance from the surface, while a definite surface charge transfer occurs from p to s orbitals. The earlier results of Wang and Freeman[34,35] violate these trends; the latter authors omitted core orbitals from their basis set, and used a minimal basis to represent the valence charge. Our results also contradict the *sp* to *d* charge transfer obtained for transition-metal surfaces by Tersoff and Falicov,[60] who used an atomic-orbital basis but parametrized the Hamiltonian matrix elements. This discrepancy has important implications for the magnetic behavior (for example, the magnetic moment is closely related to the number of *d* holes) as well as the catalytic activity of these surfaces.[61] In later applications of the parametrized LCAO method, Tersoff and Falicov[62] imposed the constraint that n_{sp} and n_d not differ from the bulk values. With this constraint they found the surface magnetic moment of Ni(100) to be $0.74\mu_B$, 32% larger than the (fitted) bulk moment $0.56\mu_B$. The surface-moment enhancement we obtained, 8%, is substantially smaller than that of Ref. 62; other first-principles results[36,37] are also smaller, 7% and 19%, relative to the center-plane moments. The surface states and resonances reported in Ref. 62 are in reasonable agreement with the first-principles calculations, although the exchange splitting is overestimated since correlation effects are omitted.

The DOS's we computed are narrowed at the surface, due to the reduced coordination. Orbitals whose lobes are directed out of the surface plane have the largest effect; the narrowing and shifting of the corresponding bands leads to a triangular appearance of the surface DOS's. For each of the films, the majority-spin bands are narrower than the minority-spin bands since the exchange potential is deeper. The exchange splittings are largest near E_F due to bonding effects.

Our use of atomic orbitals made possible an assessment of the causes of the ESM as well as the constancy of n_d. By repeating the calculations with the *sp-d* matrix elements set equal to zero, the effects of dehybridization and *sp*-band narrowing were separated. We found that dehybridization at the surface makes a minor contribution to the ESM of nickel films. Instead, the magnetic moment is closely related to the *sp*-band occupancy, which increases

TABLE IX. Orbital occupation numbers and magnetic moments of Ni(100) monolayers with lattice spacings of $0.9a$, $1.0a$, and $1.2a$. These values were obtained using the Löwdin projection technique (Ref. 48).

Lattice spacing	n_s	n_p	n_d	m (μ_B)
$0.9a$	0.78	0.37	8.79	0.80
$1.0a$	0.89	0.30	8.77	0.98
$1.2a$	1.05	0.17	8.76	1.08

TABLE X. Orbital occupation numbers and magnetic moments of Ni(100) monolayers, obtained by setting *sp-d* hybridization matrix elements equal to zero. f_d is the ratio n_d/n_d^0.

Lattice spacing	n_{sp}^0	n_d^0	m^0 (μ_B)	$n_{d\uparrow}^0$	f_d
0.9a	0.95	9.01	0.81	4.91	0.976
1.0a	1.02	8.95	1.06	5.00	0.980
1.2a	1.12	8.86	1.15	4.99	0.988

at the surface due to band narrowing. Dehybridization, which increases the *d* character of the *nominal d* bands at the surface, does explain why the *d*-orbital occupation number is nearly constant: The increase of n_d is canceled by the decrease caused by *sp*-band narrowing.

The effects of dehybridization and *sp*-band narrowing were also studied by expanding and contracting the nickel monolayer. We found that n_d remains almost unchanged, while a charge transfer occurs from *p* to *s* orbitals as the lattice parameter is increased. The magnetic moment increases as the monolayer is expanded because the number of *d*-band holes increases. The magnetism of the contracted film is reduced due to the creation of $d\uparrow$-band holes as well as band broadening. Hybridization effects are rather weak in all three monolayers, due to the reduced coordination.

We found a $\bar{\Sigma}_2$ surface-state band which may explain surface bands mapped out by angle-resolved photoemission spectroscopy[14,16] near $\bar{\Gamma}$ and $\bar{M}$. No even-parity minority-spin surface band was obtained near $\bar{X}$ which could explain a surface-sensitive band observed by Plummer and Eberhardt.[14] The observed state may be a bulk majority-spin state with slightly enhanced surface amplitude.

ACKNOWLEDGMENTS

This work was supported in part by the National Science Foundation MONTS-NSF project No. ISP-80-11449 at Montana State University (MSU), Bozeman, Montana. One of us (R.R.) was partially supported by a stipend from MSU.

[1]U. Baenninger, G. Busch, M. Campagna, and H. C. Siegmann, Phys. Rev. Lett. 25, 585 (1970); D. T. Pierce and H. C. Siegmann, Phys. Rev. B 9, 4035 (1974).
[2]W. Eib and S. F. Alvarado, Phys. Rev. Lett. 37, 444 (1976).
[3]E. Kisker, W. Gudat, E. Kuhlmann, R. Clauberg, and M. Campagna, Phys. Rev. Lett. 45, 2053 (1980).
[4]R. J. Celotta, D. T. Pierce, G.-C. Wang, S. D. Bader, and G. P. Felcher, Phys. Rev. Lett. 43, 728 (1979).
[5]H. C. Siegmann, Phys. Rev. B 17, 37 (1975); M. Landholt and M. Campagna, Phys. Rev. Lett. 38, 663 (1977).
[6]P. M. Tedrow and R. Meservey, Phys. Rev. B 7, 318 (1973).
[7]C. Rau, Comments Solid State Phys. 9, 177 (1980); C. Rau and S. Eichner, Phys. Rev. Lett. 47, 939 (1981).
[8]G. Bergmann, Phys. Rev. Lett. 41, 264 (1978); Phys. Today 32(4), 25 (1979).
[9]W. Goepel, Surf. Sci. 85, 400 (1979).
[10]D. W. Gidley, A. R. Koymen, and T. W. Capehart, Phys. Rev. Lett. 49, 1779 (1982).
[11]E. Dietz, U. Gerhardt, and C. J. Maetz, Phys. Rev. Lett. 40, 892 (1978).
[12]D. E. Eastman, F. J. Himpsel, and J. A. Knapp, Phys. Rev. Lett. 40, 1514 (1978); F. J. Himpsel, J. A. Knapp, and D. E. Eastman, Phys. Rev. B 19, 2919 (1979); D. E. Eastman, F. J. Himpsel, and J. A. Knapp, Phys. Rev. Lett. 44, 95 (1980).
[13]P. Heimann and H. Neddermeyer, J. Magn. Magn. Mater. 15-18, 1143 (1980).
[14]E. W. Plummer and W. Eberhardt, Phys. Rev. B 20, 1444 (1979).
[15]W. Eberhardt, E. W. Plummer, K. Horn, and J. Erskine, Phys. Rev. Lett. 45, 273 (1980).
[16]J. L. Erskine, Phys. Rev. Lett. 45, 1446 (1980).
[17]L. Gonzales, R. Miranda, M. Salmeron, J. A. Verges, and F. Yndurain, Phys. Rev. B 24, 3245 (1981).
[18]F. J. Himpsel and Th. Fauster, Phys. Rev. B 26, 2679 (1982); D. P. Woodruff, N. V. Smith, P. D. Johnson, and W. A. Roger, *ibid.* 26, 2943 (1982).
[19]J. Unguris, A. Seiber, R. J. Celotta, and D. T. Pierce, Phys. Rev. Lett. 49, 1047 (1982).
[20]U. von Barth and L. Hedin, J. Phys. C 5, 1629 (1972).
[21]O. Gunnarson, B. I. Lundqvist, and S. Lundqvist, Solid State Commun. 11, 149 (1972); O. Gunnarson and B. I. Lundqvist, Phys. Rev. B 13, 4274 (1976).
[22]A. K. Rajagopal and J. Callaway, Phys. Rev. B 7, 1912 (1973).
[23]J. W. D. Connolly, Phys. Rev. 159, 415 (1967).
[24]C. S. Wang and J. Callaway, Phys. Rev. B 15, 298 (1977).
[25]V. L. Moruzzi, J. F. Janak, and A. R. Williams, *Calculated Electronic Properties of Metals* (Pergamon, New York, 1978).
[26]J. R. Anderson, D. A. Papaconstantopoulos, L. L. Boyer, and J. E. Schirber, Phys. Rev. B 20, 3172 (1979).
[27]D. M. Ceperley, Phys. Rev. B 18, 3126 (1978); D. M. Ceperley and B. J. Alder, Phys. Rev. Lett. 45, 566 (1980).
[28]S. H. Vosko, L. Wilk, and M. Nusair, Can. J. Phys. 58, 1200 (1980).
[29]D. R. Penn, Phys. Rev. Lett. 42, 921 (1979).
[30]L. A. Feldkamp and L. C. Davis, Phys. Rev. Lett. 43, 151 (1979); L. C. Davis and L. A. Feldkamp, J. Appl. Phys. 50, 1944 (1979); Solid State Commun. 34, 141 (1980).
[31]A. Liebsch, Phys. Rev. Lett. 43, 1431 (1979); Phys. Rev. B 23, 5203 (1981).
[32]L. Kleinman, Phys. Rev. B 19, 1295 (1979); L. Kleinman and

K. Mednick, *ibid.* 24, 6880 (1981).
[33]G. Treglia, F. Ducastelle, and D. Spanjaard, Phys. Rev. B 22, 6472 (1980).
[34]C. S. Wang and A. J. Freeman, J. Appl. Phys. 50, 1940 (1979); Phys. Rev. B 21, 4585 (1980).
[35]C. S. Wang and A. J. Freeman, Phys. Rev. B 19, 793 (1979).
[36]O. Jepsen, J. Madsen, and O. K. Andersen, Phys. Rev. B 26, 2790 (1982).
[37]H. Krakauer, A. J. Freeman, and E. Wimmer, Phys. Rev. B 28, 610 (1983). Very similar results were obtained using the full-potential LAPW method; see A. J. Freeman, H. Krakauer, S. Ohnishi, D.-S. Wang, M. Weinert, and E. Wimmer, J. Phys. (Paris) 43, C7-167 (1982) and A. J. Freeman, J. Magn. Magn. Mater. 35, 31 (1983).
[38]O. Jepsen, J. Madsen, and O. K. Andersen, Phys. Rev. B 18, 605 (1978).
[39]J. Noffke and L. Fritsche, J. Phys. C 14, 89 (1981).
[40]J. R. Smith, J. G. Gay, and F. J. Arlinghaus, Phys. Rev. B 21, 2201 (1980).
[41]J. G. Gay, J. R. Smith, and F. J. Arlinghaus, Phys. Rev. B 25, 643 (1982), and references therein.
[42]Xue-yuan Zhu and J. Hermanson, Phys. Rev. B 27, 2092 (1983).
[43]Harrison Shull and Per-Olov Löwdin, J. Chem. Phys. 30, 617 (1959).
[44]F. J. Arlinghaus, J. R. Smith, J. G. Gay, and R. Richter, Phys. Rev. B 27, 6507 (1983).
[45]E. Wimmer, H. Krakauer, M. Weinert, and A. J. Freeman, Phys. Rev. B 24, 864 (1981); B. Delley, A. J. Freeman, M. Weinert, and E. Wimmer, *ibid.* 27, 6509 (1983).
[46]D. J. Chadi and M. L. Cohen, Phys. Rev. B 8, 5747 (1973); S. J. Cunningham, *ibid.* 10, 4988 (1974).
[47]R. S. Mulliken, J. Chem. Phys. 23, 1833 (1955).
[48]P. O. Löwdin, J. Chem. Phys. 18, 365 (1950).
[49]C. A. Papageorgopoulos and J. M. Chen, Surf. Sci. 52, 40 (1975).
[50]F. J. Arlinghaus, J. G. Gay, and J. R. Smith, Phys. Rev. B 21, 2055 (1980).
[51]G. P. Alldredge and L. Kleinman, Phys. Rev. B 10, 559 (1974). Our x and y axes here are parallel to the sides of the square surface unit cell. This is in contrast to the convention adopted in Ref. 42, where the bulk coordinate system was used.
[52]J. Hermanson, Solid State Commun. 22, 9 (1977).
[53]I. Tamm, Z. Phys. 76, 849 (1932).
[54]P. Heimann, J. Hermanson, H. Miosga, and H. Neddermeyer, Phys. Rev. B 20, 3059 (1979).
[55]D. G. Dempsey and L. Kleinman, Phys. Rev. Lett. 39, 1297 (1977); D. G. Dempsey, W. R. Grise, and L. Kleinman, Phys. Rev. B 18, 1270 (1978).
[56]I. D. Moore and J. B. Pendry, J. Phys. C 11, 4615 (1978).
[57]D. M. Bylander, L. Kleinman, and K. Mednick, Phys. Rev. B 25, 1090 (1982).
[58]J. Harris and R. O. Jones, J. Chem. Phys. 68, 3316 (1978).
[59]J. P. Perdew and A. Zunger, Phys. Rev. 23, 5048 (1981).
[60]J. Tersoff and L. M. Falicov, Phys. Rev. B 24, 754 (1981).
[61]L. Kleinman, Phys. Rev. B 26, 1055 (1982).
[62]J. Tersoff and L. M. Falicov, Phys. Rev. B 26, 6186 (1982).